Chemical Science

ROYAL SOCIETY OF CHEMISTRY

EDGE ARTICLE

View Article Online
View Journal | View Issue

Check for updates

Cite this: *Chem. Sci.*, 2020, **11**, 6752

All publication charges for this article have been paid for by the Royal Society of Chemistry

An aromatic micelle with bent pentacene-based panels: encapsulation of perylene bisimide dyes and graphene nanosheets†

Kenta Ito, Tomoya Nishioka, Munetaka Akita, Akiyoshi Kuzume, Kimihisa Yamamoto and Michito Yoshizawa *

Received 26th March 2020
Accepted 4th June 2020

DOI: 10.1039/d0sc01748e

rsc.li/chemical-science

For exploitation of a new class of aromatic micelles, we synthesized a bent pentacene-based amphiphilic molecule through Diels–Alder reaction. The amphiphiles bearing two trimethylammonium tethers assemble into a spherical aromatic micelle, with an average core diameter of 1.5 nm, in water at room temperature. The new aromatic micelle efficiently encapsulates perylene bisimide (PBI) dyes and graphene nanosheets (GNS) in water. The encapsulated PBI dyes form a parallel stacked dimer, exhibiting characteristic absorption and emission bands. In addition, the encapsulated GNS are composed of few-layer graphene sheets with an average lateral size of ~7 nm, as confirmed by Raman spectroscopy. The resultant, aqueous host–guest complexes are stable even after three weeks in water under ambient conditions.

Introduction

Polyacenes provide planar π-electron-rich frameworks with unique photo/electrochemical properties, like typical polyaromatic compounds (*e.g.*, pyrene and perylene).[1] On the other hand, unlike other polyaromatics, their tape-shaped frameworks display characteristic reactivities: the central benzene rings can be easily and selectively functionalized from the side edges or face (Fig. 1a). Pentacene is one of the most appealing polyacenes. Its edge-functionalization has been intensively investigated for the development of advanced photofunctional materials (*e.g.*, chemical sensors, thin film transistors, and solar cells).[2,3] However, pentacene-based components, synthesized *via* face-functionalization, usable for supramolecular systems have been rarely explored so far, despite the facile accessibility by Diels–Alder reaction.[4] We thus employed pentacene as a starting material for the design of new face-functionalized, amphiphilic molecule **PA** (Fig. 1b), capable of forming an aqueous supramolecular container with intriguing host functions.[5,6] Here we report the formation of aromatic micelle $(\mathbf{PA})_n$ from bent pentacene-based amphiphiles **PA** with two trimethylammonium tethers in water at room temperature and its unusual host abilities toward relatively large perylene bisimide (PBI) dyes[7] and graphene nanosheets (GNS) in water.[8] In the new host cavity, the encapsulated PBI dyes form a parallel stacked dimer, exhibiting characteristic spectral bands and the encapsulated GNS comprise few-layer sheets with small lateral size (~7 nm), as confirmed by Raman analysis. The resultant, host–guest complexes remain intact in water under ambient conditions even after three weeks.

Recently, we have shown that anthracene-based amphiphiles **AA** (Fig. 1d) with bent dianthrylbenzene frameworks assemble into well-defined, spherical micelles in water through π-stacking interactions and the hydrophobic effect.[9] The bent amphiphile is synthesized *via* Pd-catalyzed cross-coupling reaction (*i.e.*, edge-functionalization) using 9-bromoanthracene.

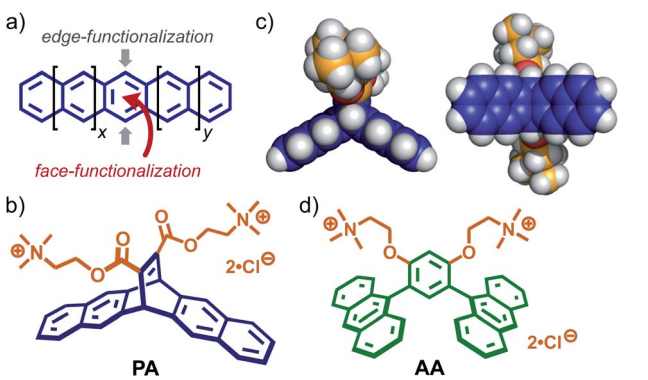

Fig. 1 (a) Schematic representation of the edge- and face-functionalization of a polyacene. (b) Bent pentacene-based amphiphilic molecule **PA**, designed in this work and (c) its optimized structure (side and bottom views). The optimized structure of **PA** was obtained by DFT calculations (B3LYP/6-31G (d) level, Gaussian 16 Rev A.03).[12] (d) Anthracene-based amphiphile **AA**.

Laboratory for Chemistry and Life Science, Institute of Innovative Research, Tokyo Institute of Technology, 4259 Nagatsuta, Midori-ku, Yokohama 226-8503, Japan. E-mail: yoshizawa.m.ac@m.titech.ac.jp

† Electronic supplementary information (ESI) available. See DOI: 10.1039/d0sc01748e

Obtained aromatic micelle $(\mathbf{AA})_n$ possesses a flexible aromatic cavity capable of binding a wide range of hydrophobic compounds (*e.g.*, fullerenes and carbon nanotubes) in water.[6b,10] In contrast to the previous amphiphile, bent pentacene-based amphiphile **PA** (Fig. 1b) designed herein provides the following three features. (i) The bent aromatic framework is constructed by the transition metal-free and 100% atom-economic Diels–Alder reaction of pentacene and a dienophile. (ii) The framework with a dihedral angle of 120° has a hydrophobic pocket on the concave side (Fig. 1c, left). (iii) Two hydrophilic groups, attached on the convex side, adopt an orthogonal orientation with respect to the bent aromatic framework, facilitating efficient π-stacking interactions (Fig. 1c, right). Although the Diels–Alder reaction is a very simple and useful synthetic tool, its use for the preparation of supramolecular capsules has been limited so far.[5,6,11]

Results and discussion

Formation of a bent pentacene-based micelle

New amphiphile **PA**, synthesized in five steps, assembled into aromatic micelle $(\mathbf{PA})_n$ in water in a spontaneous and quantitative manner. The Diels–Alder reaction of pentacene and dimethyl acetylenedicarboxylate gave rise to a hydrophobic, bent pentacene framework in 62% yield. The subsequent transformation of the methyl groups into hydrophilic trimethylammonium groups afforded **PA**, whose monomeric structure was confirmed by NMR and MS analyses (Fig. S1–S14†).[12] Once a white solid of **PA** (6.4 mg, 10 μmol) was added to water (0.5 mL) at room temperature, aromatic micelle $(\mathbf{PA})_n$ was quantitatively formed within 1 min through π-stacking interactions and the hydrophobic effect (Fig. 2a). In ^{1}H NMR spectra, upon formation of $(\mathbf{PA})_n$ in D_2O (20.0 mM based on **PA**), the bent pentacene signals H_c and H_d of **PA** were remarkably shifted upfield as compared with those observed in CD_3OD ($\Delta\delta = -0.49$ and −0.44 ppm, respectively; Fig. 2b and c). The average size (core diameter) of the product was estimated to be 1.5 nm by DOSY NMR (Fig. 2d) and DLS analyses (Fig. 2e).[13] Molecular modeling studies suggested that the size corresponds well to that of spherical pentamer $(\mathbf{PA})_5$, featuring the average core and outer diameters of ∼1.6 and ∼2.6 nm, respectively (Fig. 2f).

The concentration-dependent ^{1}H NMR and DLS studies of $(\mathbf{PA})_n$ in water indicated the critical micelle concentration (CMC) being <∼20 mM based on **PA** (Fig. S18 and S20†). Unlike the similar UV-visible absorption bands of $(\mathbf{PA})_n$ and **PA**, the fluorescence band of **PA** (λ_{max} = 343 nm in methanol) was largely bathochromically shifted ($\Delta\lambda$ = +33 nm) upon micelle formation (20.0 mM based on **PA** in water; Fig. S19†).

Encapsulation of perylene bisimide dyes

To explore the characteristic host functions of aromatic micelle $(\mathbf{PA})_n$, we focused on perylene bisimides (PBIs), which are an important class of organic dyes frequently employed as supramolecular building blocks,[7] exhibiting strong absorption bands in the visible region. Without directing groups, the planar core frameworks of the PBI dyes usually aggregate randomly in the solid state as well as in aqueous solution. 3,5-Dimethylphenyl-substituted perylene bisimide **PBI-1**, known as Pigment Red 149, is insoluble in water and hardly soluble in common organic solvents (*e.g.*, $CHCl_3$, acetone, and DMSO) owing to its strong aggregation. Nevertheless, aromatic micelle $(\mathbf{PA})_n$ could readily solubilize **PBI-1** in water at room temperature upon encapsulation. As an optimized protocol, red solid **PBI-1** was ground with amphiphile **PA** in a 1 : 2 molar ratio for 5 min using a small mortar and pestle. After sequential water addition, centrifugation, and filtration, host–guest complex $(\mathbf{PA})_n\cdot(\mathbf{PBI\text{-}1})_m$ was

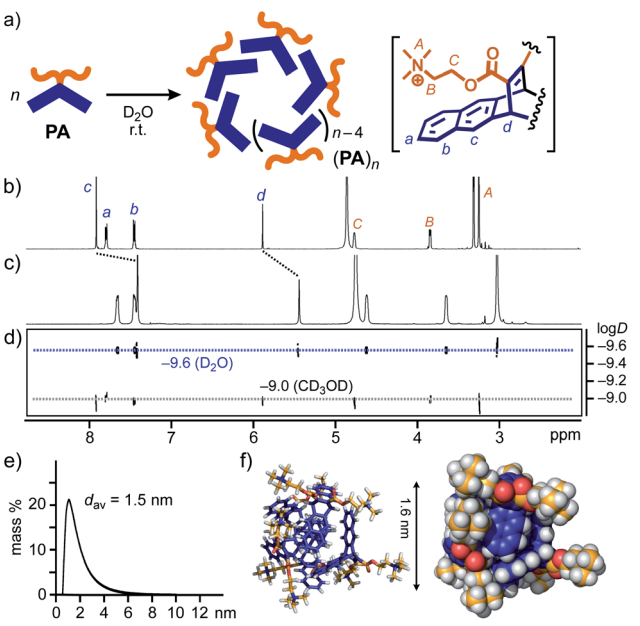

Fig. 2 (a) Schematic representation of the formation of aromatic micelle $(\mathbf{PA})_n$ from amphiphile **PA** in water. ^{1}H NMR spectra (500 MHz, r.t.) of (b) **PA** in CD_3OD and (c) $(\mathbf{PA})_n$ in D_2O (20 mM based on **PA**), and (d) their DOSY NMR spectra (500 MHz, 25 °C). (e) DLS chart (H_2O, r.t.) and (f) optimized structure (n = 5) of $(\mathbf{PA})_n$. The optimized structure was obtained by molecular mechanics (MM) calculations (Forcite module, Materials Studio, ver. 5.5.3).[12]

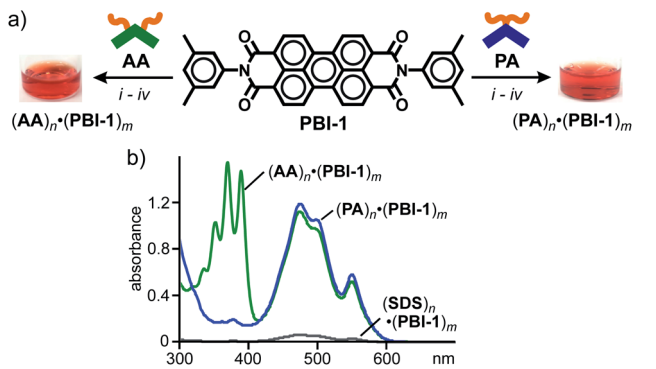

Fig. 3 (a) Encapsulation of **PBI-1** dyes by amphiphiles **PA** and **AA** in water and the photographs of the resultant solutions. Procedures: (i) manual grinding (5 min), (ii) water addition, (iii) high-speed centrifugation (16 000*g*, ∼10 min), and (iv) membrane filtration (200 nm in pore size). (b) UV-visible spectra (H_2O, r.t., 1.0 mM based on the amphiphiles) of $(\mathbf{PA})_n\cdot(\mathbf{PBI\text{-}1})_m$, $(\mathbf{AA})_n\cdot(\mathbf{PBI\text{-}1})_m$, and $(\mathbf{SDS})_n\cdot(\mathbf{PBI\text{-}1})_m$.

obtained as a clear, red aqueous solution (Fig. 3a, right).[12,14] The UV-visible spectrum showed broadened yet intense absorption bands in the range of 400 to 600 nm (Fig. 3b), which indicates the concentration of solubilized **PBI-1** in water being 0.54 mM. The absorption bands of $(\mathbf{PA})_n\cdot(\mathbf{PBI\text{-}1})_m$ are comparable to those of solid **PBI-1** (ref. 15) so that encapsulated $(\mathbf{PBI\text{-}1})_m$ dyes ($m > 2$) adopt random aggregates even within $(\mathbf{PA})_n$. The host–guest complex remains almost intact (≧96%) in water under ambient conditions even after four months (Fig. S23†).[16]

The water solubilizing ability of $(\mathbf{PA})_n$ toward **PBI-1** was compared with a typical micelle and previous aromatic micelle, consisting of linear alkane-based amphiphile, sodium dodecylsulfonate (**SDS**), and bent anthracene-based amphiphile **AA** (Fig. 1d), respectively. The treatment of **PBI-1** with **SDS** in the same way afforded a pale red solution with very weak absorption bands for $(\mathbf{PBI\text{-}1})_m$ within $(\mathbf{SDS})_n$. On the basis of the band intensity of the encapsulated dyes at 473 nm, the water solubilization of **PBI-1** by **PA** was estimated to be 17 times higher than that by **SDS**, most probably due to the efficient host–guest π-stacking interactions. An apparent red solution including $(\mathbf{AA})_n\cdot(\mathbf{PBI\text{-}1})_m$ was also obtained from **AA** and **PBI-1** (Fig. 3a, left). In the UV-visible spectra, the observed guest bands were virtually overlapped with those of $(\mathbf{PA})_n\cdot(\mathbf{PBI\text{-}1})_m$ (Fig. 3b) and thus **PA** and **AA** exhibit an equal water solubilizing ability toward **PBI-1**.[17]

In sharp contrast to $(\mathbf{PBI\text{-}1})_m$ within aromatic micelles $(\mathbf{PA})_n$ and $(\mathbf{AA})_n$, sterically demanding, 2,6-diisopropylphenyl-substituted perylene bisimide **PBI-2**, known as Perylene Orange, displayed host-dependent spectroscopic features in water at room temperature. In a manner similar to $(\mathbf{PA})_n\cdot(\mathbf{PBI\text{-}1})_m$, aqueous host–guest complex $(\mathbf{PA})_n\cdot(\mathbf{PBI\text{-}2})_m$ was formed through the grinding protocol using **PA** and **PBI-2** (Fig. 4a, right). The resultant red solution showed relatively sharp absorption bands with slight bathochromic shifts ($\Delta\lambda_{max} = +9$ nm) relative to those of **PBI-2** in CH_2Cl_2 (Fig. 4b), indicating multiple stacks of the dyes. The formation of the stacked $(\mathbf{PBI\text{-}2})_m$ species was further confirmed by a significant bathochromic shift ($\Delta\lambda = +108$ nm) of the emission band of **PBI-2** upon encapsulation (Fig. 4c). It is worthy of note that the same protocol employing **AA** and **PBI-2** generated a red purple aqueous solution of $(\mathbf{AA})_n\cdot(\mathbf{PBI\text{-}2})_m$ with broadened absorption bands in the range of 420 to 670 nm (Fig. 4a, left and Fig. 4b). The fluorescence spectrum of the resultant host–guest complex showed a couple of broad emission bands with significant bathochromic shifts (Fig. 4c). Therefore, the stacking conformation of $(\mathbf{PBI\text{-}2})_m$ and its spectroscopic properties could be modulated upon encapsulation by the aromatic micelles in water.

To gain structural insights into $(\mathbf{PA})_n\cdot(\mathbf{PBI\text{-}2})_m$, the product composition and size were revealed by NMR and DLS analyses. After lyophilization of the aqueous $(\mathbf{PA})_n\cdot(\mathbf{PBI\text{-}2})_m$ solution, the average **PA** : **PBI-2** ratio was determined to be 3 : 1 by integration of the sharp ^{1}H NMR signals of the product mixture in DMSO-d_6 (Fig. S26†). The DLS analysis of $(\mathbf{PA})_n\cdot(\mathbf{PBI\text{-}2})_m$ suggested an average diameter of 2.0 nm for the product (Fig. 4d). The combination of the obtained NMR and DLS data as well as the spectroscopic findings (Fig. 4b and c) indicates the selective formation of a $(\mathbf{PA})_6\cdot(\mathbf{PBI\text{-}2})_2$ complex, in which the parallel stacked $(\mathbf{PBI\text{-}2})_2$ are surrounded by the bent pentacene panels of $(\mathbf{PA})_6$.[7] The optimized structure bearing the hydrophobic guest core and an amphiphilic host shell provides an average core diameter of ~2 nm (Fig. 4e).

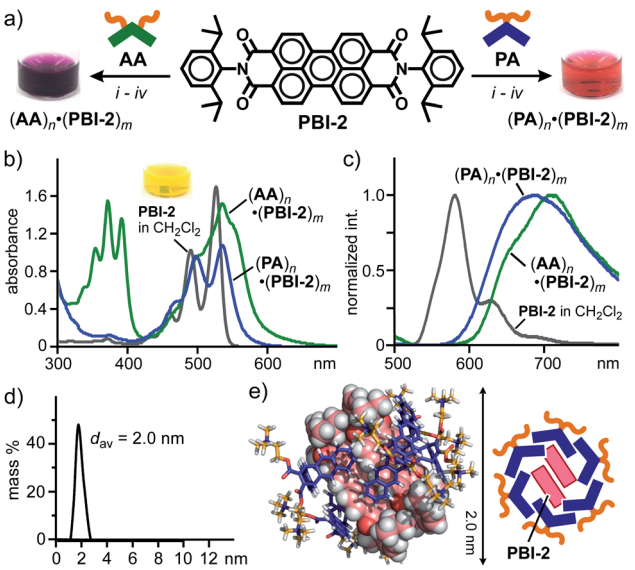

Fig. 4 (a) Encapsulation of PBI-2 dyes by amphiphiles PA and AA in water and the photographs of the resultant solutions. Procedures: (i) manual grinding (5 min), (ii) water addition, (iii) high-speed centrifugation, and (iv) membrane filtration. (b) UV-visible and (c) fluorescence spectra (H_2O, r.t., 1.0 mM based on the amphiphiles, $\lambda_{ex} = 498$ nm) of $(\mathbf{PA})_n\cdot(\mathbf{PBI\text{-}2})_m$ and $(\mathbf{AA})_n\cdot(\mathbf{PBI\text{-}2})_m$. (d) DLS chart ($H_2O$, r.t.) and (e) optimized structure ($n = 6$, $m = 2$) of $(\mathbf{PA})_n\cdot(\mathbf{PBI\text{-}2})_m$. The optimized structure was obtained by MM calculations (Forcite module).[12]

Encapsulation of fullerene and graphene nanosheets

We next investigated the host functions of $(\mathbf{PA})_n$ toward fullerene C_{60} ($\mathbf{C_{60}}$) and graphene nanosheets as typical and uncommon nanocarbon guests, respectively.[18] Anthracene-based amphiphile **AA** has been revealed to be a superior water-solubilizing agent for various fullerenes upon encapsulation.[14a] Similar solubilizing ability of **PA** was found toward $\mathbf{C_{60}}$. Simply grinding a mixture of **PA** and $\mathbf{C_{60}}$ (2 : 1 molar ratio) for

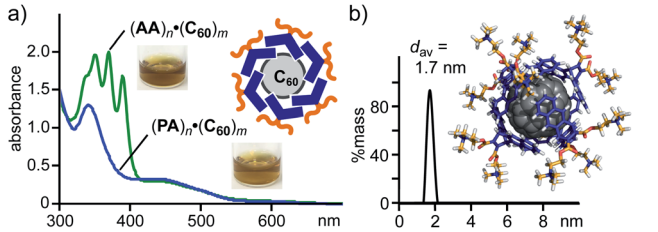

Fig. 5 (a) UV-visible spectra (H_2O, r.t., 1.0 mM based on PA or AA) and the photographs of $(\mathbf{PA})_n\cdot(\mathbf{C_{60}})_m$ and $(\mathbf{AA})_n\cdot(\mathbf{C_{60}})_m$. (b) DLS chart ($H_2O$, 1.0 mM based on PA, r.t.) of $(\mathbf{PA})_n\cdot(\mathbf{C_{60}})_m$ and optimized structure of $(\mathbf{PA})_6\cdot\mathbf{C_{60}}$. The optimized structure was obtained by MM calculations (Forcite module).[12]

5 min and subsequent addition of water to the resultant solid generated a brown aqueous solution of host–guest complex $(\mathbf{PA})_n\cdot(\mathbf{C_{60}})_m$. After removal of the excess guest, the UV-visible spectrum of the product solution showed clear absorption bands assignable to encapsulated $(\mathbf{C_{60}})_m$ around 340 and 450 nm (Fig. 5a). The band intensity is comparable to that of $(\mathbf{AA})_n\cdot(\mathbf{C_{60}})_m$ prepared in the same way. The amphiphile-fullerene ratio ($n = 6$, $m = 1$) and size (1.7 nm in core diameter) of $(\mathbf{PA})_n\cdot(\mathbf{C_{60}})_m$ were confirmed by UV-visible and DLS analyses (Fig. 5b).

The encapsulation test for well-defined fullerene prompted us to examine the encapsulation and water-solubilization of large nanocarbon sheets with various dimensions by pentacene-based micelle $(\mathbf{PA})_n$. Graphene nanosheets (**GNS**) employed here are multilayer sheets in a platelet morphology (2–10 nm in thickness and 5 μm in width), which are sparingly soluble in water using additives (*e.g.*, **SDS** and sodium dodecylbenzenesulfonate).[12,18] The combination of grinding and sonication operations with **PA** enabled the efficient formation of host–guest complex $(\mathbf{PA})_n\cdot$**GNS** in water (Fig. 6a, right). A mixture of **PA** (0.6 mg, 1.0 μmol) and **GNS** (0.3 mg) was ground for 5 min and the resultant black solid was sonicated in H_2O (1.0 mL) for 10 min at room temperature. The high-speed centrifugation (16 000*g* for 30 min) and membrane filtration (200 nm in pore size) of the obtained suspension gave a clear black aqueous solution.[12] The UV-visible-NIR, DLS, and Raman analyses of the black solution revealed the formation of $(\mathbf{PA})_n\cdot$**GNS**. The UV-visible-NIR spectrum displayed wide-ranging, very broadened absorption bands without characteristic peaks, derived from encapsulated **GNS** (Fig. 6b). The high stability of the host–guest structure was clarified by the absorption spectrum after three weeks (Fig. S32†). The DLS chart showed a single peak with an average diameter of 5.2 nm and a relatively narrow size distribution (Fig. 6c), suggesting the selective encapsulation of small graphene sheets.

Notably, water-solubilizing ability of $(\mathbf{PA})_n$ toward **GNS** was higher than that of $(\mathbf{AA})_n$ and $(\mathbf{SDS})_n$. The same grinding and sonication protocols using **AA** and **SDS** instead of **PA** yielded black and colorless solutions, respectively, showing very broadened absorption bands in the UV-visible-NIR spectra (Fig. 6a and b). The band intensities of encapsulated **GNS** (at 660 nm) indicate that the water solubilizing ability of **PA** is 1.4- and 18-fold higher than that of **AA** and **SDS**, respectively. The observed, high solubilizing ability of **PA** most probably arises from efficient π-stacking interactions between the bent pentacene framework and the graphene surface (Fig. S35†). The concentration of **GNS** in the resultant $(\mathbf{PA})_n\cdot$**GNS** solution (1.0 mM based on **PA**) was calculated at 0.18 mg mL^{-1}.[12] In a manner similar to $(\mathbf{PA})_n\cdot$**GNS**, a black aqueous solution of $(\mathbf{PA})_n\cdot$**SG** was efficiently obtained using **PA** and synthetic graphite (**SG**; 10 μm in average size).[12] The UV-visible-NIR spectrum and DLS chart of the product (Fig. 6b and c) resembles those of $(\mathbf{PA})_n\cdot$**GNS**, assuming the incorporation of small graphene sheets into the micelle cavity in water.

Finally, the detailed structures of **GNS** and **SG** within aromatic micelle $(\mathbf{PA})_n$ were elucidated by Raman spectroscopic analysis. The Raman spectrum of $(\mathbf{PA})_n\cdot$**GNS** (532 nm laser wavelength) exhibited clear peaks at 1348, 1584, 1623, and 2692 cm^{-1}, corresponding to the typical D, G, D′, and 2D bands of graphenes, respectively (Fig. 7a), in Raman-inactive water at room temperature. On the basis of the ratio of the observed D and G band intensities (*i.e.*, $I_D/I_G = 2.62$), the lateral guest size of $(\mathbf{PA})_n\cdot$**GNS** was estimated to be 7.3 nm (Fig. 7e).[12,19a] The shape and position of the observed 2D band indicate the presence of few-layer graphene sheets, particularly monolayer sheets as a major component.[19b,c] The relatively large peak width (*i.e.*, full width at half maximum (FWHM) = 62 cm^{-1}) of the 2D band agrees with the presence of defect-rich graphene sheets and

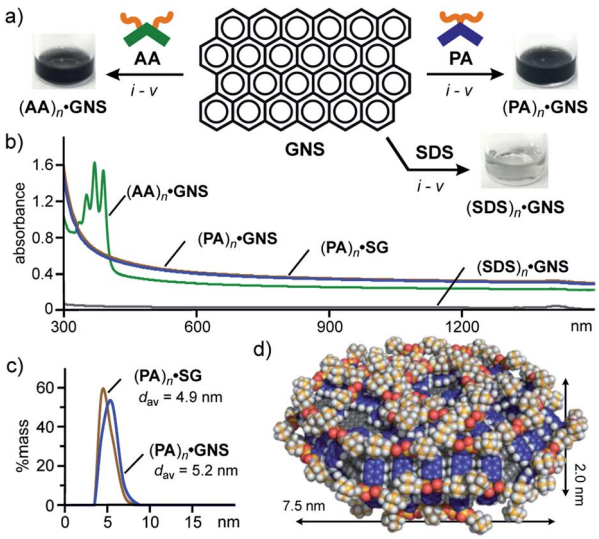

Fig. 6 (a) Schematic representation of the encapsulation of **GNS** by amphiphiles **PA**, **AA**, and **SDS** in water and the photographs of the resultant solutions. Procedures: (i) manual grinding (5 min), (ii) water addition, (iii) sonication (40 kHz, 10 min), (iv) high-speed centrifugation (16 000*g*, ~30 min), and (v) membrane filtration (200 nm in pore size). (b) UV-visible-NIR spectra (H_2O, r.t., 1.0 mM based on the amphiphiles) of $(\mathbf{PA})_n\cdot$**GNS**, $(\mathbf{AA})_n\cdot$**GNS**, $(\mathbf{PA})_n\cdot$**SG**, and $(\mathbf{SDS})_n\cdot$**GNS**. (c) DLS charts (H_2O, r.t.) and (d) optimized structure ($n = 66$, 3-layer graphene sheet) of $(\mathbf{PA})_n\cdot$**GNS**. The optimized structure was obtained by MM calculations (Forcite module).[12]

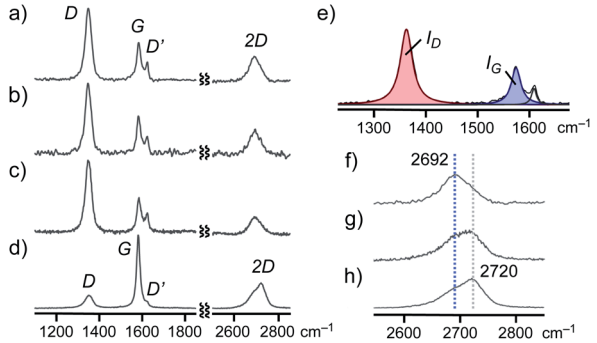

Fig. 7 Raman spectra (H_2O, DPSS laser, $\lambda = 532$ nm, r.t.) of (a) $(\mathbf{PA})_n\cdot$**GNS**, (b) $(\mathbf{AA})_n\cdot$**GNS**, (c) $(\mathbf{PA})_n\cdot$**SG**, and (d) **GNS** (solid). (e) Expanded and its deconvoluted D and G bands of $(\mathbf{PA})_n\cdot$**GNS**. Raman spectra (H_2O, $\lambda = 532$ nm, r.t.) of the expanded 2D bands of (f) $(\mathbf{PA})_n\cdot$**GNS**, (g) ground and sonicated **GNS** (solid), and (h) pristine **GNS** (solid).

thus indicates the formation of the small graphene sheets (Fig. 7f). The combination of the present Raman data with the UV-visible-NIR and DLS findings concluded that aromatic micelle $(\mathbf{PA})_n$ could efficiently exfoliate and encapsulate the few-layer nanosheets of **GNS** through simple grinding and sonication protocols.

The Raman spectra of $(\mathbf{AA})_n\cdot\mathbf{GNS}$ (Fig. 7b) and $(\mathbf{PA})_n\cdot\mathbf{SG}$ (Fig. 7c) in water also indicated the exfoliation and encapsulation of similar graphene sheets (6.9 and 6.1 nm in lateral size, respectively; Table S1†) by the aromatic micelles. It is worth noting that the Raman analysis of a pristine **GNS** sample, bearing large lateral size (*e.g.*, $I_D/I_G = \sim 0.4$; Fig. 7d and S40†) and wide-ranging thickness, remains almost unchanged after sequential grinding (5 min) and sonicating (30 min) in the absence of **PA** (Fig. 7f–h). Accordingly, aromatic micelle $(\mathbf{PA})_n$ captured small graphene sheets (1–3 layers) in a selective fashion from a complex mixture of **GNS** (Fig. 6d).

Conclusions

We have designed and synthesized a bent pentacene-based amphiphilic molecule through Diels–Alder reaction as a key face-functionalization step. The amphiphiles spontaneously and quantitatively assemble into a spherical aromatic micelle (~2 nm in diameter) in water at room temperature. The new class of aromatic micelles displays efficient encapsulation abilities toward relatively large perylene bisimide (PBI) dyes and graphene nanosheets (GNS) in water. The resultant, highly water-soluble and stable host–guest complexes accommodate the parallel stacked dimer of a bulky PBI dye and small few-layer nanosheets of GNS, respectively, in a selective fashion. As relevant challenges and future prospects, thanks to the non-covalent host–guest interactions, the encapsulated PBI and GNS guests could potentially be released from the host cavity,[14b] which prompts us to develop novel functional solid materials through the present, pentacene-based aromatic micelle.

Conflicts of interest

There are no conflicts to declare.

Acknowledgements

M. Y. acknowledges the financial support from JSPS KAKENHI (Grant No. JP17H05359/JP18H01990/JP19H04566) and "Support for Tokyo Tech Advanced Researchers (STAR)". A. K. and K. Y. also acknowledge the financial support from JST ERATO (Grant No. JPMJER1503).

Notes and references

1 (*a*) J. E. Anthony, *Chem. Rev.*, 2006, **106**, 5028–5048; (*b*) J. E. Anthony, *Angew. Chem., Int. Ed.*, 2008, **47**, 452–483.

2 (*a*) D. Lehnherr and R. R. Tykwinski, *Materials*, 2010, **3**, 2772–2800; (*b*) C. Hetzer, D. M. Guldi and R. R. Tykwinski, *Chem.–Eur. J.*, 2018, **24**, 8245–8257; (*c*) K. Kuroda, K. Yazaki, Y. Tanaka, M. Akita, H. Sakai, T. Hasobe, N. V. Tkachenko and M. Yoshizawa, *Angew. Chem., Int. Ed.*, 2019, **58**, 1115–1119.

3 *Physics and Chemistry of Carbon-Based Materials: Basics and Applications*, ed. Y. Kubozono, Springer, 2019, ch. 7.

4 (*a*) A. Afzali, C. D. Dimitrakopoulos and T. L. Breen, *J. Am. Chem. Soc.*, 2002, **124**, 8812–8813; (*b*) D. F. Perepichka, M. Bendikov, H. Meng and F. Wudl, *J. Am. Chem. Soc.*, 2003, **125**, 10190–10191; (*c*) R. M. Tromp, A. Afzali, M. Freitag, D. B. Mitzi and Z. Chen, *Nano Lett.*, 2008, **8**, 469–472.

5 Reviews on aqueous supramolecular containers: (*a*) G. V. Oshovsky, D. N. Reinhoudt and W. Verboom, *Angew. Chem., Int. Ed.*, 2007, **46**, 2366–2393; (*b*) M. Yoshizawa, J. K. Klosterman and M. Fujita, *Angew. Chem., Int. Ed.*, 2009, **48**, 3418–3438; (*c*) J. H. Jordan and B. C. Gibb, *Chem. Soc. Rev.*, 2015, **44**, 547–585; (*d*) J. Murray, K. Kim, T. Ogoshi, W. Yaod and B. C. Gibb, *Chem. Soc. Rev.*, 2017, **46**, 2479–2496.

6 Reviews on aromatic micelles: (*a*) W. Li, Y. Kim and M. Lee, *Nanoscale*, 2013, **5**, 7711–7723; (*b*) K. Kondo, J. K. Klosterman and M. Yoshizawa, *Chem.–Eur. J.*, 2017, **23**, 16710–16721.

7 (*a*) F. Würthner, *Chem. Commun.*, 2004, 1564–1579; (*b*) A. Nowak-Król and F. Würthner, *Org. Chem. Front.*, 2019, **6**, 1272–1318.

8 (*a*) Y. Zhu, S. Murali, W. Cai, X. Li, J. W. Suk, J. R. Potts and R. S. Ruoff, *Adv. Mater.*, 2010, **22**, 3906–3924; (*b*) K. S. Novoselov, V. I. Fal'ko, L. Colombo, P. R. Gellert, M. G. Schwab and K. Kim, *Nature*, 2012, **490**, 192–200; (*c*) T. Kuila, S. Bose, A. K. Mishra, P. Khanra, N. H. Kim and J. H. Lee, *Prog. Mater. Sci.*, 2012, **57**, 1061–1105.

9 (*a*) K. Kondo, A. Suzuki, M. Akita and M. Yoshizawa, *Angew. Chem., Int. Ed.*, 2013, **52**, 2308–2312; (*b*) Y. Okazawa, K. Kondo, M. Akita and M. Yoshizawa, *J. Am. Chem. Soc.*, 2015, **137**, 98–101; (*c*) L. Catti, N. Kishida, T. Kai, M. Akita and M. Yoshizawa, *Nat. Commun.*, 2019, **10**, 1948; (*d*) Y. Satoh, L. Catti, M. Akita and M. Yoshizawa, *J. Am. Chem. Soc.*, 2019, **141**, 12268–12273.

10 M. Yoshizawa and L. Catti, *Acc. Chem. Res.*, 2019, **52**, 2392–2404.

11 (*a*) R. S. Meissner, J. de Mendoza and J. Rebek, Jr., *Science*, 1995, **270**, 1485–1488; (*b*) G. H. Clever, S. Tashiro and M. Shionoya, *Angew. Chem., Int. Ed.*, 2009, **48**, 7010–7012; (*c*) M. D. Johnstone, E. K. Schwarze, G. H. Clever and F. M. Pfeffer, *Chem.–Eur. J.*, 2015, **21**, 3948–3955.

12 See the ESI.† For the sample preparation, the initial molar ratio of **PA** and the guest (for grinding) is important to efficiently obtain the corresponding host–guest complex. Simple grinding for approximately 5 min is enough for guests $\mathbf{C_{60}}$, **PBI-1**, and **PBI-2**. On the other hand, the combination of ~5 min grinding and ~10 min sonication is essential for highly hydrophobic guests **GNS** and **SG**.

13 The DOSY NMR spectrum of $(\mathbf{PA})_n$ in D_2O displayed a single band at $D = 2.5 \times 10^{-10}$ m^2 s^{-1}, which is smaller than that of **PA** in CD_3OD (8.3×10^{-10} m^2 s^{-1}, Fig. 2d). The core diameter of $(\mathbf{PA})_n$ was calculated on the basis of the D value and the Stokes–Einstein equation.

14 (*a*) K. Kondo, M. A. T. Nakagawa, Y. Matsuo and M. Yoshizawa, *Chem.–Eur. J.*, 2015, **21**, 12741–12746; (*b*) K. Kondo, M. Akita and M. Yoshizawa, *Chem.–Eur. J.*, 2016, **22**, 1937–1940.

15 J. Mizuguchi and K. Tojo, *J. Phys. Chem. B*, 2002, **106**, 767–772.

16 Whereas guest-free aromatic micelle $(\mathbf{PA})_n$ was very sensitive to the concentration, the host–guest complexes were insensitive to the concentration (up to ~0.1 mM), because of efficient host–guest hydrophobic effect and π–π/CH–π interactions, in water.

17 Another representative organic dye, Nile Red (**NR**) was also efficiently encapsulated by $(\mathbf{PA})_n$ and $(\mathbf{AA})_n$ in water by the same grinding protocol. The absorption bands derived from $(\mathbf{NR})_m$ within $(\mathbf{PA})_n$ are almost comparable to those within $(\mathbf{AA})_n$ (Fig. S22b†).

18 (*a*) M. Lotya, Y. Hernandez, P. J. King, R. J. Smith, V. Nicolosi, L. S. Karlsson, F. M. Blighe, S. De, Z. Wang, I. T. McGovern, G. S. Duesberg and J. N. Coleman, *J. Am. Chem. Soc.*, 2009, **131**, 3611–3620; (*b*) V. Georgakilas, J. N. Tiwari, K. C. Kemp, J. A. Perman, A. B. Bourlinos, K. S. Kim and R. Zboril, *Chem. Rev.*, 2016, **116**, 5464–5519.

19 (*a*) L. G. Cançado, K. Takai, T. Enoki, M. Endo, Y. A. Kim, H. Mizusaki, A. Jorio, L. N. Coelho, R. Magalhães-Paniago and M. A. Pimenta, *Appl. Phys. Lett.*, 2006, **88**, 163106; (*b*) L. G. Cançado, A. Reina, J. Kong and M. S. Dresselhaus, *Phys. Rev. B*, 2008, **77**, 245408; (*c*) L. M. Malard, M. A. Pimenta, G. Dresselhaus and M. S. Dresselhaus, *Phys. Rep.*, 2009, **473**, 51–87.